

System Design and Analysis for Energy-Efficient Passive UAV Radar Imaging System using Illuminators of Opportunity

Zhichao Sun, *Member, IEEE*, Junjie Wu, *Member, IEEE*, Gary G. Yen, *Fellow, IEEE*, Hang Ren, *Student Member, IEEE*, Hongyang An, *Student Member, IEEE*, Jianyu Yang, *Member, IEEE*

arXiv:2010.00179v1 [eess.SP] 1 Oct 2020

Abstract—Unmanned aerial vehicle (UAV) can provide superior flexibility and cost-efficiency for modern radar imaging systems, which is an ideal platform for advanced remote sensing applications using synthetic aperture radar (SAR) technology. In this paper, an energy-efficient passive UAV radar imaging system using illuminators of opportunity is first proposed and investigated. Equipped with a SAR receiver, the UAV platform passively reuses the backscattered signal of the target scene from an external illuminator, such as SAR satellite, GNSS or ground-based stationary commercial illuminators, and achieves bi-static SAR imaging and data communication. The system can provide instant accessibility to the radar image of the interested targets with enhanced platform concealment, which is an essential tool for stealth observation and scene monitoring. The mission concept and system block diagram are first presented with justifications on the advantages of the system. Then, the prospective imaging performance and system feasibility are analyzed for the typical illuminators based on signal and spatial resolution model. With different illuminators, the proposed system can achieve distinct imaging performance, which offers more alternatives for various mission requirements. A set of mission performance evaluators is established to quantitatively assess the capability of the system in a comprehensive manner, including UAV navigation, passive SAR imaging and communication. Finally, the validity of the proposed performance evaluators are verified by numerical simulations.

Index Terms—synthetic aperture radar, unmanned aerial vehicle, illuminators of opportunity, system concept, energy efficient.

I. INTRODUCTION

Synthetic aperture radar (SAR) is capable of high-resolution imaging in all-day and all-weather environments [1]–[3], which has been proven to be an indispensable sensor for modern remote sensing applications, such as military reconnaissance, flight navigation, disaster monitoring and geological mapping, etc. In recent years, various aspects of SAR technology have been extensively studied, including bi/multi-static SAR [4]–[6], interferometry and polarimetry measurement

Z. Sun, J. Wu, H. Ren, H. An and Jianyu Yang are with School of Information and Communication Engineering, University of Electronic Science and Technology of China, Chengdu, People's Republic of China, 611731 (e-mail:threadkite@sina.com).

G. G. Yen is with the School of Electrical and Computer Engineering, Oklahoma State University, Stillwater, MN 74078 USA (e-mail:gyen@okstate.edu).

This work was supported in part by the National Natural Science Foundation of China under Grant 61901088, Grant 61922023, Grant 61771113, and Grant 61801099, in part by the Postdoctoral Innovation Talent Support Program under Grant BX20180059, and in part by the China Postdoctoral Science Foundation under Grant 2019M65338 and Grant 2019TQ0052.

[7]–[9], data focusing methods [10], [11] and moving target indication [12], [13]. Moreover, SAR sensors can be mounted on different platforms in order to satisfy distinct remote sensing and mission requirements, including spaceborne [14]–[16], airborne [17], [18] and missile-borne [19]–[21] platforms.

Compared with other platforms, unmanned aerial vehicles (UAVs) provide better mission safety and maneuverability with less cost [22]–[24], which has been widely used in advanced application scenarios [25]–[31]. The SAR systems mounted on UAV platforms have been intensively studied in the current literature, including system design [32]–[34], performance analysis [35], [36], imaging methods [37], [38] and motion compensation [39]–[41]. Instead of using its own illuminator, a SAR radar can use an illuminator of opportunity, which is not originally designed for SAR imaging purposes, forming a passive SAR. Consequently, passive SAR allows for silent operations, which can in turn enhance the system survivability in military scenarios. Moreover, due to the lack of transmitter, the system cost, weight and energy consumption can be greatly reduced compared with the active SAR counterpart, which is suitable for light-weight UAV platforms. In view of these advantages, plenty of researches have been undertaken on passive SAR imaging technology [42]–[45]. In [46], a passive SAR system with airborne receiver using DVB-T illumination was investigated. Signal processing techniques were discussed and experiments were conducted to validate the system feasibility. On the other hand, bistatic UAV SAR system using external illuminator was investigated in [47], [48], where the UAV platform passively received the backscattered signal from a GEO-SAR illuminator. The system performance and path planning were also analyzed in detail.

This paper proposes an energy-efficient passive UAV radar imaging system using illuminators of opportunity, which combines the UAV SAR and passive SAR technology. In this paper, the system and mission concept are first put forward with discussions on the application benefits. The system block diagram is also given to specify the main component of the UAV receiver. By passively receiving the signal of an external illuminator, such as spaceborne SAR satellite, GNSS and DVB-T illuminators, the UAV platform then sends the echo data to a ground processing station after onboard preprocessing and synchronization, where image formation and target recognition are further accomplished. The prospective imaging performance, feasibility and imaging method are analyzed based on spatial geometry, signal and resolution modeling.

It is found that different system performance can be achieved by exploiting various types of illuminators. Then, the mission performance of the passive UAV SAR system is analyzed in detail. A set of mission performance is established to quantitatively assess the performance of the system, which comprehensively considers the three main aspects, *i.e.* UAV navigation, SAR imaging and communication. The proposed evaluator set offers the theoretical foundation for optimizing the mission performance of the energy-efficient passive UAV radar imaging system by dynamically adapting the adopted UAV path in 3-D terrain environments, which will be our future work.

The main contributions of this paper can be summarized as follows.

- In this paper, an energy-efficient passive UAV SAR system is put forward. The system concept, main components and advantages are specified, which can serve as a potential technical alternative for advanced remote sensing applications and future SAR systems.
- The feasibility and characteristics of the passive UAV SAR system with different illuminators are analyzed in detail. By exploiting various types of illuminators, the UAV platform can achieve the mission goal with different imaging and beam coverage performance, which offers more flexibility for mission planning.
- The mission performance of the system with respect to UAV path in 3-D terrain environments are thoroughly analyzed in detail, including navigation, radar imaging and communication. The energy consumption model for UAV in 3-D motion and the spatial resolution model for target scene are derived for the first time in 3-D UAV path planning.
- A set of mission performance evaluators is proposed to quantitatively assess the overall capability of the system. Numerical simulations are conducted to verify the validity of the evaluator set, which lays the theoretical foundation for mission planning of the system.

The rest of the paper is organized as follows. Section II introduces the system and mission concepts, advantages and block diagram of the proposed energy-efficient passive UAV SAR system. Section III first presents the signal and spatial resolution models based on imaging geometry. Then, the prospective imaging performance and feasibility of the system is analyzed in detail, along with comparisons of different choices of illuminators. In Section IV, the mission performance of the system is derived and the performance evaluator set is established in detail, pertaining the navigation, SAR imaging and communication aspects. In Section V, simulations are carried out to verify the effectiveness of the mission performance evaluator set. Finally, conclusions are drawn in Section VI.

II. PROPOSED ENERGY-EFFICIENT PASSIVE UAV SAR SYSTEM

A. System and Mission Concept

The proposed energy-efficient passive UAV SAR utilizes transmitters of opportunity to illuminate the target scene. The

potential illuminators can be flexibly chosen from satellite-borne SAR (LEO-SAR and future GEO/MEO-SAR [15], [16]), global navigation satellite system (GNSS) or ground-based stationary commercial illuminators (*e.g.*, FM radio and DVB-T) according to their beam coverage and signal characteristics. The UAV platform passively receives the echo signal reflected from the target scene and achieves bistatic SAR imaging at a ground-based processing station.

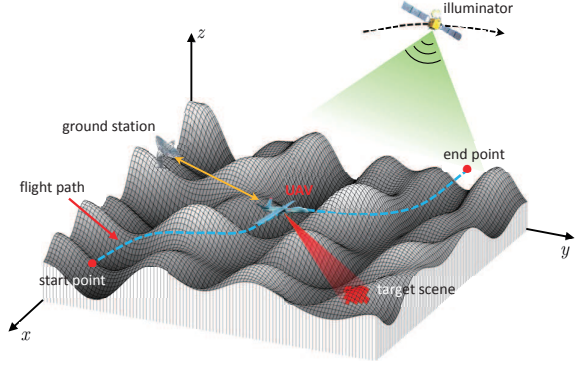


Fig. 1. A typical scenario for energy-efficient passive UAV SAR system.

The typical working scenario of the system is illustrated in Fig. 1. Without loss of generality, the interested target scene to be imaged is supposed to be located in a 3-D rough terrain, which is marked as red squares in Fig. 1. First of all, according to the geometric location of the target scene, calculate the beam coverage time and motion parameters of the illuminator based on its orbit parameters (for ground-based stationary illuminators, these parameters can be readily obtained). Then, generate an optimal flight path using the digital elevation model (DEM) information, which can safely guide the UAV to travel through the 3-D terrain and achieve passive bistatic SAR imaging and communication during the flight. The optimal path is then loaded in the navigation system and the UAV is deployed according to the time schedule and flight path. The UAV platform travels from the start point to the end point and collects echo from the target scene during a predefined time window. Finally, after on-board signal preprocessing, the echo data is transmitted to the ground-based processing station for the accurate focusing and imaging of the interested target scene.

Based on the above analysis, the proposed UAV SAR system has the following advantages.

1) By exploiting various illuminators of opportunity, the UAV SAR system can obtain different advantages contributed by the specific illuminator. For instance, GEO/MEO SAR can provide large beam coverage with long duration. The LEO-SAR illuminator can provide large range and Doppler bandwidths, which can achieve high-resolution imaging. The signal transmitted by a SAR satellite is generally linear frequency modulation (LFM) pulse and is suitable for coherent focusing. On the other hand, the GNSS and ground-based commercial illuminators are useful when frequent monitoring or persistent surveillance is desired, due to their continuous beam coverage. The illuminator can be chosen according to the mission requirements.

2) The UAV platform and the illuminator form a bistatic SAR. The imaging performance of the bistatic SAR system is closely related to the observation geometry. Therefore, the overall imaging and flight performance of the UAV SAR system can be optimized by path planning.

3) The UAV platform passively receives the signal radiated from the illuminator. Moreover, the ground processing station can be located far away from the imaged region and the transmitted power for communication is much lower than typical signal power for SAR imaging. Therefore, the proposed UAV SAR system can provide better stealth surveillance capability compared with the traditional airborne SAR.

4) The system can be equipped with miniaturized and light-weighted UAV platforms. Compared with a full-functional SAR system, the SAR signal generator and transmitter can be removed. Moreover, by moving the SAR imaging and target recognition tasks to the ground processing station, the energy consuming real-time signal processor is no longer needed in the energy-efficient passive UAV SAR system.

B. System Block Diagram

Based on the main functions described above, the block diagram of the proposed energy-efficient passive UAV SAR system is shown in Fig. 2. The system mainly consists of three functional modules, *i.e.* navigation, communication and SAR processing subsystems, which collaborates with each other to accomplish the radar imaging task.

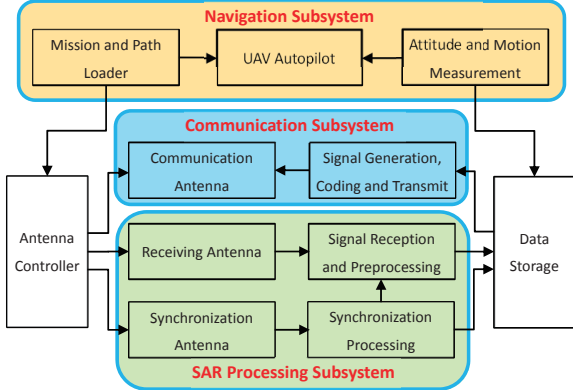


Fig. 2. The proposed block diagram of energy-efficient passive UAV SAR system.

a) Navigation Subsystem: The navigation subsystem generates pilot commands for the UAV platform according to the predefined mission, UAV path, real-time attitude and motion information.

In the mission and path loader, the mission parameters and UAV path are installed ahead of deployment. The mission parameters include the geometric locations of the target scene and ground processing station as well as motion parameters of the illuminator during data collection period. The loader provides the data required by antenna controller to generate beam pointing commands for antennas with different purposes.

The attitude and motion measurement parts contain high-precision inertial navigation system (INS) and GPS to provide

the UAV motion information, which is essential for autopilot and subsequent SAR imaging. Based on these information, the UAV autopilot component generates the real-time pilot commands for UAV flight control.

b) SAR Processing Subsystem: The SAR processing subsystem receives direct synchronization signal and echo signal reflected from the target scene. After synchronization and signal preprocessing, the data are stored in data storage for communication subsystem.

The proposed UAV SAR system is essentially a bi-static SAR and synchronization between the transmitter and receiver is required for coherent processing of SAR data. The UAV platform is equipped with two pairs of antenna dedicated to SAR processing, which correspond to two synchronous receiving channels respectively, *i.e.* reference channel and surveillance channel. For the reference channel, the beam of synchronization antenna is pointed toward the illuminator to record direct signal from the transmitter for synchronization [49], [50]. On the other hand, the receiving antenna collects echo data from the targets for observation of the interested scene. The two channels use the same clocks and local oscillators to guarantee the synchronization between them.

The signal reception contains a low-noise amplifier and a down converter to bring the received signal to an appropriate band for analog-to-digital sampling. The digital signal is then aligned in a 2-D echo data matrix and range compression is implemented using reference signal extracted from synchronization processing to reduce data volume for transmission.

c) Communication Subsystem: The communication subsystem is dedicated to transmit the echo data, synchronization information and motion parameters to the ground processing station. On-board SAR imaging processing is an energy and time consuming task. In order to promote the processing speed, high-performance signal processor is required, which takes up considerable space of the UAV platform. Moreover, after SAR imaging, target classification and recognition based on SAR image are needed for information extraction, which in turn requires more energy budget and space. For a miniaturized and light-weighted UAV platform considered in this paper, energy and space are limited resources and need careful arrangement. Therefore, in the proposed UAV SAR system, the echo data after preprocessing are transmitted to a ground processing station where the following SAR imaging and target recognition are finished. After signal generation and coding, the data are modulated to a predefined carrier and transmitted by the communication antenna, which is pointed to the ground processing station.

III. IMAGING GEOMETRY AND FEASIBILITY ANALYSIS

A. Signal Model and Spatial Resolution

As mentioned in the above section, the UAV platform receives the echo signal reflected from the target scene in a specific time interval during the flight path. Let the center point of the target scene be the reference target denoted by O . The observation geometry of the UAV SAR system at beam center crossing time of reference target is illustrated in Fig. 3.

Without loss of generality, a satellite-borne illuminator is assumed in Fig. 3, which can be chosen from GNSS or SAR

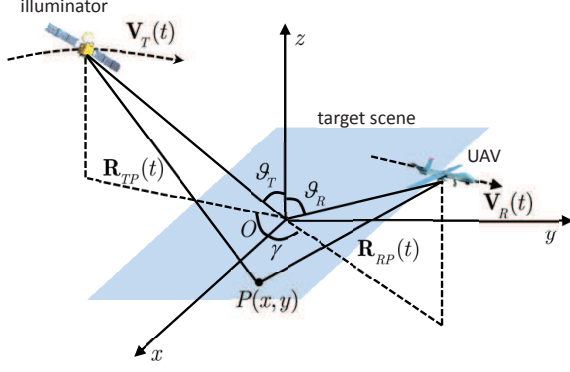


Fig. 3. Observation geometry of the proposed passive UAV SAR.

satellite. For a ground-based stationary illuminator, the motion parameters can be set as constant with respect to time t , i.e. $\mathbf{V}_T(t) = 0$ and $\mathbf{R}_{TP}(t) = \mathbf{R}_{TP}$. The shaded area represents the interested target scene to be imaged and $P(x, y)$ is an arbitrary target located in the scene. $\mathbf{V}_T(t)$ and $\mathbf{V}_R(t)$ denote the velocity of the illuminator and receiver, respectively, which are time-variant. $\mathbf{R}_{TP}(t)$ and $\mathbf{R}_{RP}(t)$ are the instantaneous slant ranges of the illuminator and receiver with respect to target P , respectively. ϑ_T and ϑ_R represent the incidence angles of the reference point. γ is the bi-static angle, which is the angle between the ground projections of the lines of sight from O to the transmitter and the receiver.

The range history of the passive UAV SAR for target P can be expressed as

$$R_{bi}^P(t) = R_{TP}(t) + R_{RP}(t), \quad (1)$$

where $R_{TP}(t)$ and $R_{RP}(t)$ represent the norm of $\mathbf{R}_{TP}(t)$ and $\mathbf{R}_{RP}(t)$, respectively. Let $S(\tau) \exp\{j2\pi f_c \tau\}$ denote the transmitted signal of the illuminator, the echo collected by receiving antenna after demodulation is given by

$$S_{rec}(t, \tau) = S(\tau - \frac{R_{bi}^P(t)}{c}) \exp\left\{-j2\pi f_c \frac{R_{bi}^P(t)}{c}\right\}, \quad (2)$$

where t and τ denote the slow time and fast time variables, respectively. c is the speed of light and f_c is the carrier frequency. On the other hand, the reference signal is extracted from the direct signal by synchronization processing and then used for range compression

$$S_{Rcomp}(t, \tau) = \int S_{rec}(t, u) S_{ref}^*(t, \tau - u) du, \quad (3)$$

where S_{ref}^* is the complex conjugate of reference signal. The above range compression can be efficiently implemented in range frequency domain by phase multiplication. The echo data size is significantly reduced by range compression. After that, the echo signal is coded and transmitted to the ground-based station for further imaging processing. In this paper, the back-projection algorithm (BPA) is applied for the accurate focusing of passive UAV SAR data. BPA is a general imaging method within high precision and high computational burden, which can be used in different imaging geometries [19], [51]. BPA can be conveniently integrated with motion compensation methods to deal with motion errors of the UAV platform.

Moreover, the processing station can provide enough computing, energy and space resources to implement BPA, which is not available on UAV platform.

Spatial resolution is a crucial parameter characterizing an imaging radar's performance. For the proposed passive UAV SAR system, the 2-D resolution can be determined by ground range resolution ρ_r^g , ground azimuth resolution ρ_a^g and resolution direction angle α_D . In order to accurately formulate the spatial resolution, the traditional gradient method [52], [53] is extended to the passive UAV SAR case, where the temporal and spatial variances of the resolution are considered. According to the gradient method, the range resolution is originated from the bi-static time delay resolution. Therefore, the gradient of time delay represents the range resolution of the SAR system. Let $\tau_P(t)$ denote the bi-static time delay of the echo signal of target $P(x, y)$, the gradient of $\tau_P(t)$ can then be formulated by partial derivatives of $\tau_P(t)$ with respect to the spatial coordinates as follows

$$\begin{aligned} \nabla \tau_P(t) &= \frac{\partial \tau_P(t)}{\partial x} \mathbf{i} + \frac{\partial \tau_P(t)}{\partial y} \mathbf{j} + \frac{\partial \tau_P(t)}{\partial z} \mathbf{k} \\ &= \frac{1}{c} [\boldsymbol{\mu}_{TP}(t) + \boldsymbol{\mu}_{RP}(t)], \end{aligned} \quad (4)$$

where \mathbf{i} , \mathbf{j} and \mathbf{k} are the unit vectors of spatial coordinates x , y and z , respectively. $\boldsymbol{\mu}_{TP}$ and $\boldsymbol{\mu}_{RP}$ are the unit vectors in the directions from target P to the transmitter and the receiver, respectively.

The ground range resolution ρ_r^g can then be written as

$$\rho_r^g(x, y; t) = \frac{k_{rg}}{B_r \|P_\tau^\perp \nabla \tau_P(t)\|}, \quad (5)$$

where B_r is the bandwidth and k_{rg} is related to the range waveform of the transmitted signal. P_τ^\perp denotes the ground projection matrix for time delay gradient. It can be observed that the ground range resolution is influenced by the system parameters as well as imaging geometry.

On the other hand, the azimuth resolution is derived from the Doppler resolution. Let $f_P(t)$ be the Doppler frequency of the echo signal for target P , its time-variant gradient can be written as

$$\nabla f_P(t) = \frac{1}{\lambda} [\omega_{TP}(t) \boldsymbol{\Gamma}_{TP}(t) + \omega_{RP}(t) \boldsymbol{\Gamma}_{RP}(t)], \quad (6)$$

where ω_{TP} and ω_{RP} are the instantaneous angular speed of the transmitter and receiver, respectively, with respect to target P . λ is the wavelength of the transmitted signal. $\boldsymbol{\Gamma}_{TP}$ and $\boldsymbol{\Gamma}_{RP}$ denote the unit vectors in the directions of rotation of the transmitter and the receiver, respectively, with respect to target P .

Different from the traditional gradient method, the angular speed and rotation direction in (6) are time-variant, which is the case for the proposed passive UAV SAR system. Therefore, the ground azimuth resolution should be formulated by integrating the Doppler gradient within synthetic aperture time T_a as follows

$$\rho_a^g(x, y; t) = \frac{k_{az}}{\int_{t-T_a/2}^{t+T_a/2} \|P_t^\perp \nabla f_P(t)\| dt}, \quad (7)$$

where k_{az} is related to the azimuth antenna pattern. P_t^\perp is the ground projection matrix for Doppler gradient.

The ground resolution direction angle can then be determined by calculating the angle between the directions of ρ_r^g and ρ_a^g .

$$\alpha_D = \cos^{-1}(\Xi \cdot \Theta), \quad (8)$$

where Ξ and Θ are the unit vectors in the resolution directions of ρ_r^g and ρ_a^g , respectively,

$$\Xi = \frac{P_\tau^\perp \nabla \tau_P(t)}{\|P_\tau^\perp \nabla \tau_P(t)\|}, \quad \Theta = \frac{P_t^\perp \nabla f_P(t)}{\|P_t^\perp \nabla f_P(t)\|}. \quad (9)$$

To comprehensively evaluate the spatial resolution, the resolution area is introduced, which is the area of the -3dB resolution cell

$$S_c = \frac{\rho_r^g \rho_a^g}{\sin \alpha_D}. \quad (10)$$

In actual application scenario of the proposed system, the UAV platform is likely to follow a curved trajectory as illustrated in Fig. 1 and the influence of time-variant motion parameters on ρ_a^g is taken into consideration by the integration within the synthetic aperture time. Moreover, from (4) to (10), it can be concluded that the spatial resolution of passive UAV SAR is related to the location of the target. Therefore, the spatial variance of resolution should be considered to accurately evaluate the imaging performance in the entire target scene.

B. Imaging Performance and Feasibility Analysis

In this subsection, the prospective imaging performance of the passive UAV SAR system with various types of illuminators are analyzed, including spatial resolution and radiometric performance.

a) Spatial resolution: Based on the above analysis, the ground range resolution can be further simplified using the geometric relations as follows

$$\rho_r^g = \frac{k_{rg} c}{2B_r \cos \frac{\vartheta}{2} \cos \vartheta}, \quad (11)$$

where ϑ is the ground projection angle of Ξ . It can be observed that ρ_r^g is bounded by the bandwidth and the finest ground range resolution is given by $k_{rg} c / 2B_r$.

On the other hand, the ground azimuth resolution in (7) needs to calculate the synthetic aperture time T_a , which is determined by the system parameters, antenna dimensions and imaging geometry. Let d_{az} and d_{el} denote the receiving antenna sizes of the UAV SAR in azimuth and elevation directions, respectively. The relation between beamwidth and antenna size can be written as

$$\beta_{az} = \frac{\lambda}{d_{az}}, \quad \beta_{el} = \frac{\lambda}{d_{el}}. \quad (12)$$

Then, T_a can be calculated as

$$T_a = \frac{\beta_{az} R_{RP}}{v_R}, \quad (13)$$

where R_{RP} is the distance between the UAV platform and target P , v_R is the speed of UAV. Based on the synthetic

aperture time in (13), the ground azimuth resolution of an arbitrary target can be determined by calculating the bi-static rotation angle θ_{biP} within T_a and (7) can be simplified as

$$\rho_a^g = \frac{k_{az} \lambda}{\theta_{biP} \cos \phi}, \quad (14)$$

where ϕ is the ground projection angle of Θ . (14) indicates that a larger rotation angle within T_a can enhance the azimuth resolution appreciably.

b) Radiometric performance: The radiometric performance of a SAR system can be characterized by the noise equivalent sigma zero (NESZ) [54], which is given by

$$NE\sigma_0 = \frac{(4\pi)^2 R_{RP}^2 k T_0 F_0 L_s}{\Phi_{PD} G_R \lambda^2 S_c T_a D_c}, \quad (15)$$

where D_c is the duty cycle, T_0 noise temperature, F_0 receiver noise factor and L_s the propagation losses. Φ_{PD} is the power density of the illuminator given by

$$\Phi_{PD} = \frac{P_T G_T}{4\pi R_{TP}^2}. \quad (16)$$

G_R is the antenna gain of the receiver as follows, which depends on the physical area of the antenna A_p and efficiency coefficient η_e

$$G_R = \frac{4\pi \eta_e A_p}{\lambda^2}. \quad (17)$$

It can be concluded that NESZ is inversely proportional to the focused SNR of the SAR image and a lower NESZ implies better radiometric sensitivity of the system.

c) Illuminator comparison and feasibility analysis: Based on the above analysis, the imaging performance of the passive UAV SAR system is significantly influenced by the signal and power characteristics of the illuminator, e.g., B_r , D_c , λ and Φ_{PD} . Therefore, the potential imaging performance with different illuminators is quantitatively analyzed and compared based on their corresponding system parameters to assess the feasibility of the proposed system.

The size requirement simulated for the receiving antenna is set as 0.5m in elevation direction and 1.2m in azimuth with rectangular shape, which is practical for general fixed-wing UAV platform. The simulated distance between UAV and target P is set as 3km, i.e. $R_{RP} = 3\text{km}$. The speed of UAV platform is $v_R = 50\text{m/s}$ and the resulting angular speed is 16.7mrad/s in side-looking mode. The noise temperature T_0 is set as 300K, the propagation losses $L_s = 3.5\text{dB}$ and receiver noise factor $F_0 = 4\text{dB}$. On the other hand, the system parameters of the illuminators being considered for the proposed system is given in Table I.

It can be observed that the illuminators considered for the passive UAV SAR system can be roughly categorized as space-borne SAR illuminators and other illuminators of opportunity. The space-borne SAR illuminator includes the LEO-SAR satellites and future MEO/GEO SAR systems, which are dedicated to monostatic/bi-static SAR imaging. SAR illuminators transmit pulsed LFM signal, which can provide large bandwidth and high compression ratio for high-resolution imaging. The power density of SAR illuminators is generally higher than those of other illuminators of opportunity, which benefits

TABLE I
SYSTEM AND SIGNAL PARAMETERS OF DIFFERENT ILLUMINATORS.

Illuminator Type	Frequency (f_c)	Bandwidth (B_r)	Duty Cycle (D_c)	Power Density (Φ_{PD})	Signal Type	Angular Speed [†] (ω_{TP})
DVB-T	750MHz	6MHz	1	-71dBW/m ²	Continuous Wave OFDM Coding	0
GNSS (Galileo)	1.19GHz	20MHz	1	-127dBW/m ²	Continuous Wave CDMA Coding	0.11mrad/s
LEO-SAR (TerraSAR-X)	9.65GHz	300MHz	0.1	-49.6dBW/m ²	Pulsed LFM	10.4mrad/s
MEO-SAR	5.4GHz	87MHz	0.08	-64.5dBW/m ²	Pulsed LFM	0.68mrad/s
GEO-SAR	1.25GHz	100MHz	0.07	-74.3dBW/m ²	Pulsed LFM	0.06mrad/s

[†]45° incidence angle assumed.

the focused SNR and radiometric performance of the UAV SAR. For the illuminators of opportunity, DVB-T and GNSS systems are considered, which adopt continuous wave coding signal. Originally designed for navigation and communication purposes, these systems generally provide smaller bandwidth than that of SAR illuminator, which limits the achievable spatial resolution [42], [43]. Another problem is that the coded format will disturb the phase of the azimuth signal and deteriorate compression performance, which coarsens the azimuth resolution.

For the DVB-T illuminator, the finest achievable ground range resolution is 25m with 6MHz bandwidth, where $k_{rg} = 1$ is assumed. As DVB-T transmitter is stationary, the azimuth resolution is contributed solely by the UAV receiver, of which the upper bound is approximately 1.2m. Owing to the low carrier frequency, the azimuth beamwidth is the largest among the illuminators with the same d_{az} and the estimated synthetic aperture time is 20s. Moreover, the receiving antenna gain is approximately 13.7dB, using the assumed antenna size and efficiency coefficient $\eta_e = 0.5$. Therefore, the NESZ of the UAV SAR system with DVB-T illuminator is -67.3dB. For the GNSS illuminator, the largest bandwidth available is 20MHz using the Galileo E5 signal, which provides finest ρ_r^g of 7.5m. Inspecting Table I, the angular speed of GNSS satellite is much smaller compared with that of UAV platform and the azimuth resolution is mainly contributed by the receiver. Therefore, the azimuth resolution of UAV SAR is 1.19m, which is similar to that of DVB-T illuminator. However, due to the comparatively low power density of the transmitted signal of GNSS system, the NESZ of the UAV SAR system with GNSS illuminator is -4.1dB in 12.6s synthetic aperture time, which can not ensure a high enough focused SNR in the final SAR image. Methods to enhance the received signal power and radiometric performance of passive SAR using GNSS illuminator have been studied [55], [56], e.g., increasing the accumulation time T_a and combining the signal energy of multiple GNSS satellites which simultaneously illuminate the same area.

On the other hand, the satellite SAR illuminators can provide finer spatial resolution compared with other illuminators. In Table I, the TerraSAR-X satellite is assumed for LEO-SAR, of which the orbit altitude is 514km [14]. According to the current literature, the orbit altitude of MEO-SAR is set as 5,952km and high inclination GEO-SAR is considered

in the simulation [15], [16]. The finest ρ_r^g are 0.5m, 1.72m and 1.5m and the ground azimuth resolution ρ_a^g are 0.73m, 1.15m and 1.19m for the simulated LEO-SAR, MEO-SAR and GEO-SAR illuminator, respectively. The NESZ of the system with LEO-SAR illuminator is -48.5dB, -42.3dB for MEO-SAR illuminator and -38dB for GEO-SAR illuminator, which are much lower than -22dB to ensure a satisfactory radiometric performance for the passive UAV SAR system [54].

It can be concluded from the above analysis that SAR satellites can generally provide better spatial resolution and radiometric performance, which are promising illuminator for UAV receiver. Among the SAR illuminators, the LEO-SAR can provide the best imaging performance. However, due to the low altitude and high speed of LEO-SAR, the beam coverage performance is compromised and spatial synchronization is more difficult. In contrast, MEO/GEO SAR offers different trade-off solutions between imaging performance and beam coverage. For instance, GEO-SAR can provide wide-swath continuous beam coverage up to 6 hours for a specific target scene for hot spot monitoring applications. On the other hand, due to the ubiquitous signal coverage, DVB-T and GNSS illuminators can provide better accessibility compared with SAR satellite, which is valuable for emergency response and continuous observation.

IV. MISSION PERFORMANCE EVALUATOR

The potential imaging performance of the passive UAV SAR system is analyzed based on the parameters of the illuminator and UAV platform in the above section. For a specific UAV SAR imaging task, the mission design process can be briefly divided into the following procedures. Firstly, the desired imaging performance is determined according to the mission requirements, e.g., spatial resolution, focused SNR and imaging swath. Then, choose a suitable illuminator that can satisfy the mission requirements and identify its orbit, motion and beam coverage parameters. For instance, if the mission requires high-resolution imaging for the interested scene with $2m \times 2m$ resolution and SNR higher than 20dB, a SAR illuminator can be considered. On the other hand, a GNSS or DVB-T illuminator should be utilized if the interested scene needs to be revisited multiple times within a few hours for multi-pass interferometry and deformation measurement. After the illuminator selection, the geometric

locations of the start point, end point and ground processing station are determined considering their relative positions with respect to the interested target scene. Finally, generate the optimal path and deploy the UAV to accomplish the flight mission.

Among the mission design procedures, the most important is the optimal path planning for UAV SAR. It can be inferred from Fig. 1 that the flight safety and relative positions of the UAV with the target scene and ground processing station are dependent on the UAV path, which determines the overall mission performance of the system, including UAV navigation, imaging and communication performance. In this section, the above mission performance are analyzed and formulated with respect to UAV path in detail, which is the foundation for optimal path planning. In the following analysis, the continuous UAV path is modeled as a series of discrete path segments with N_{dp} discrete points denoted as $(P_1, \dots, P_i, \dots, P_{N_{dp}})$. The 3-D terrain is also discretized into N_g terrain mesh grid points for ease of analysis.

A. UAV Navigation and Flight Performance

UAV navigation and flight performance are the first to be considered for UAV path planning. Current literature [47], [57], [58] generally adopts path length and threat value to represent the navigation performance [59]. A smaller path length is desired to shorten the overall flight time of UAV platform, which reduce the exposure of UAV to potential air-defense radar and possibility of being detected. The distance between the UAV platform and restricted area (or terrain mesh grid points in 3-D terrain cases) is generally utilized to represent the threat value, which is minimized to guarantee the safety of UAV.

In this paper, energy consumption of UAV path in 3-D motion is derived to represent the flight performance instead of path length. In practice, the voyage range of UAV platform is usually limited by the onboard fuel capacity. Lengthen the flight path will inevitably increase energy consumption. However, maneuvering and climbing in the UAV path will bring additional energy consumption, which is not considered in path length. For instance, for two UAV paths with the same path length and threat value, the 'smoother' one with less abrupt maneuvers and climbing is preferred. Therefore, the energy consumption of UAV path is a more practical and comprehensive evaluator for UAV navigation and flight performance.

For the proposed passive UAV SAR system, the total energy consumption includes the following three parts.

(1) UAV flight control, *i.e.*, the propulsion energy needed for the UAV to travel from the start point to the end point with necessary mobility.

(2) SAR signal processing, *i.e.*, the energy for SAR processing subsystem, including synchronization, preprocessing of SAR echo and corresponding antenna control and data storage.

(3) Data communication, *i.e.*, the energy required for processing and transmitting the SAR and synchronization data to the ground processing station.

Note that in practice, the energy consumption of communication and SAR processing subsystems are much smaller than that of UAV flight control. Therefore, the power budgets of the two subsystems can be treated as constant, which is pre-allocated. On the other hand, the energy consumption of UAV flight control is the main part and is dependent on the adopted flight path, which should be analyzed in detail.

In this paper, the UAV platform is assumed to be flying in a 3-D terrain environment, which may require turning, climbing and descending. The propulsion force of fixed-wing UAV engaged in 3-D motion is analyzed in Appendix A, which is the foundation for energy consumption analysis of UAV path. For an arbitrary UAV flight path $d(t)$, the velocity \vec{v} and acceleration \vec{a} at any time instant t can be obtained by taking first and second order derivatives of $d(t)$ with respect to t . Therefore, the centrifugal acceleration a_{\perp} and flight-direction acceleration a_{\parallel} in Appendix A can be represented as

$$a_{\perp} = \sqrt{\|\vec{a}\|^2 - \left(\frac{\vec{a}^T \vec{v}}{\|\vec{v}\|}\right)^2}, \quad a_{\parallel} = \frac{\vec{a}^T \vec{v}}{\|\vec{v}\|}. \quad (18)$$

According to Appendix A, the instantaneous power required for banked level turn and climbing can be calculated by multiplying the thrust in (A.7) and speed \vec{v} , which is given by

$$P_{UAV} = |F| \vec{v} = |P_{drag} + mg \sin \gamma \|\vec{v}\| + m \vec{a}^T \vec{v}|, \quad (19)$$

where P_{drag} is the power needed to overcome drag.

$$P_{drag} = c_1 \|\vec{v}\|^3 + \frac{c_2}{\|\vec{v}\|} \left(\frac{v_a^2}{\|\vec{v}\|^2} + \frac{\|\vec{a}\|^2 - \left(\frac{\vec{a}^T \vec{v}}{\|\vec{v}\|}\right)^2}{g^2} \right). \quad (20)$$

In this paper, the UAV path is discretized as N_{dp} way points jointly denoted as $d(i), i = 1, 2, \dots, N_{dp}$. The total energy consumption of an arbitrary UAV flight path $d(i)$ can be approximated by the sum of energy consumption during each discrete path segment.

$$E(d(i)) = \sum_{i=1}^{N_{dp}-1} (P_{drag}(i)T(i) + mg [h(P_{i+1}) - h(P_i)]) + \sum_{i=1}^{N_{dp}-1} \left(\frac{1}{2} m \left[\|v(P_{i+1})\|^2 - \|v(P_i)\|^2 \right] \right), \quad (21)$$

where $h(P_i)$ is the UAV height at P_i and $T(i)$ is the time required for UAV to travel from P_i to P_{i+1} . The first term in (21) represents the energy consumption to overcome drag force, which is dependent on the velocity and centrifugal acceleration of the UAV during the flight. Moreover, compared with the conclusion in [60], P_{drag} is also influenced by the ratio of horizontal speed to actual UAV speed $v_a / \|\vec{v}\|$, which is incurred by the climbing angle γ in 3-D flight path scenario. If the UAV is engaged in level flight without vertical motion, *i.e.* $\gamma = 0$, we have $v_a / \|\vec{v}\| = 1$ and the energy consumption expression required to overcome drag is the same as that in [60]. The second term is the gravitational potential energy, denoted as ΔE_p , which is determined by the UAV mass and change of height during a specific time period. For

each discrete path segment, ΔE_p depends on the initial and final height $h(P_i)$ and $h(P_{i+1})$. The third term represents the kinetic energy, which is determined by the flight speed of UAV at initial and final positions.

Based on the above analysis, it can be concluded that a UAV path with ascending and speeding trajectory generally consumes more energy than a uniform speed and level flight path. Moreover, the total energy consumption is highly dependent on the adopted UAV path, which offers the opportunity of optimizing the energy consumption performance and achieving energy-efficient flight mission by optimizing UAV path.

In addition to the energy consumption performance, safety navigation of the flight path for passive UAV SAR should be considered in 3-D terrain scenario path planning. In this paper, we adopt the threat value in [47] to represent the safety performance of a flight path, which is given by

$$f_{\text{threat}}(d(i)) = \sum_{i=1}^{N_{dp}} \sum_{j=1}^{N_{gj}} (r_{\text{safe}}/r_{i,j})^2, \quad (22)$$

where r_{safe} is the minimum safe distance between UAV and terrain boundary, which should be set larger than the physical size of the UAV and terrain topology error to ensure safety of the UAV. $r_{i,j}$ is the distance between P_i and the j th terrain mesh point. N_{gj} is the number of discrete terrain points engaged in the calculation of the threat value of P_i . Please refer to [47] for detailed calculation of N_{gj} . On the other hand, the path should be subject to two constraints regarding UAV navigation performance. Firstly, the number of discrete way points below the terrain mesh point, denoted as N_{c1} , should be zero to avoid collision. Secondly, the turning angle between adjacent path segments should be no larger than a predefined allowable angle θ_{\max} considering the actual maneuverability of the UAV platform.

B. Passive UAV SAR Imaging Performance

Passive SAR imaging is a crucial part of mission performance evaluator. Different from [47] where spatial resolution of the scene center is the only imaging performance evaluator, in this paper, imaging swath width, spatial resolution and data size are considered to comprehensively evaluate the performance of the proposed passive UAV SAR system in practical applications.

For a passive UAV SAR mission, the desired imaging swath width is determined by the mission requirement and interested target type to be observed, e.g., vehicle, building and farmland. In Fig. 4, the azimuth swath width, denoted as W_a , can be obtained by adjusting the length of signal collecting window onboard the UAV platform. However, the range beam coverage depends on the wavelength, antenna size and receiver slant range given by

$$W_r^{\text{Cov}} = R_{RP} \beta_{el} = \frac{\lambda R_{RP}}{d_{el}}. \quad (23)$$

Range beam coverage W_r^{Cov} should be larger than the desired range swath width W_r to ensure the echo of the interested target scene are completely collected, i.e., $W_r^{\text{Cov}} \geq W_r$. It should be noted that W_r^{Cov} is determined by the flight path of

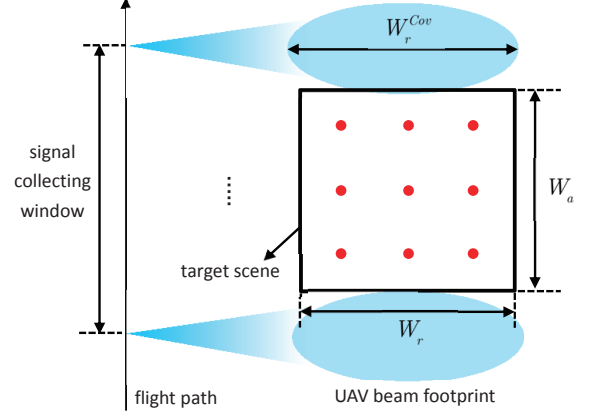


Fig. 4. Illustration of imaging swath and spatial resolution for target scene.

the UAV. Enough distance between the UAV and target scene should be maintained to achieve the desired range swath width.

According to Section III, the spatial resolution of the passive UAV SAR system changes with geometric location of the targets. The resolution cell area of the reference target can not fully represent the resolution performance of the entire target scene. Therefore, a modified resolution evaluator is proposed based on S_c , where the spatial variance of resolution is considered.

Firstly, the interested target scene with swath size $W_r \times W_a$ is discretized and N_s point targets are sampled from target scene, which are marked as red dots in Fig. 4. The N_s sampled target points are evenly distributed in the imaging scene with constant distance between adjacent targets both in azimuth and range directions. It can be inferred from (4) to (10) that the resolution cell area S_c is continuously changing with the target position. Therefore, each sampled point can represent the resolution performance of the targets in its vicinity without significant degradation. Then, the resolution cell area of the sampled points are calculated and the modified resolution evaluator can be formulated as

$$\bar{S}_c(d(i)) = \frac{S_c^{\max}}{S_c^{\min}} \cdot \frac{1}{N_s} \sum_{j=1}^{N_s} S_c^j, \quad (24)$$

where S_c^j is the S_c of the j th sampled point. S_c^{\max} and S_c^{\min} are the maximum and minimum S_c among the N_s sampled points, respectively. In (24), the first part is disequilibrium factor, i.e. the ratio of S_c^{\max} to S_c^{\min} , which represents the uniformity of the distribution of resolution performance. Larger disequilibrium factor indicates greater spatial variance of resolution performance. In practice, a uniform distribution of resolution, i.e., $S_c^{\max}/S_c^{\min} = 1$, within the imaging scene is generally desired to avoid image distortion and facilitate target recognition [61]. The second part is the mean resolution cell area of the target scene. It should be noted that the calculation of \bar{S}_c involves the motion parameters of the UAV, which depends on the adopted flight path. Therefore, the imaging performance should be considered in the path planning for passive UAV SAR.

On the other hand, the number of sampled target points N_s is directly related to the accuracy of \bar{S}_c . Larger N_s can

improve the precision of resolution evaluation at the cost of higher computational burden. Thus, a suitable N_s should be selected during path planning.

As mentioned in Section II, the echo and synchronization data are transmitted to the ground processing station for further imaging and target recognition. The synchronization data involves the 3-D positions of the illuminator and UAV platform during signal collecting window and time/frequency synchronization information, which is far less than echo data and are arguably neglected in the following analysis.

For a SAR system, the received signal after digitization is stored in a 2-D echo data matrix. The size of echo matrix to be transmitted by the communication subsystem can be calculated using the scene size and system parameters. The azimuth data size corresponds to the number of pulses received within the signal collecting window. Based on the beam coverage geometry in Fig. 4, the size of echo data matrix in azimuth direction can be represented as

$$N_a = (W_a/v + T_a) \cdot PRF, \quad (25)$$

where PRF is the pulse repetition frequency. In (25), N_a is the sum of two components. W_a/v is the time needed for UAV beam footprint to travel through the interested target scene. The second term T_a is the total time required for beam footprint to enter and exit the scene.

The range data size, on the other hand, can be calculated by the bi-static slant range variation ΔR_{bi} within W_r as follows

$$N_r = (\Delta R_{bi}/c + T_r) \cdot S_{rate}, \quad (26)$$

where T_r is the pulse width and S_{rate} is range sampling rate. ΔR_{bi} is determined by the difference between the maximum and minimum bi-static slant ranges corresponding to ground swath size of $W_a \times W_r$. After signal collection, range pulse compression is implemented before transmission to concentrate the energy of the pulse and achieve range focusing. Therefore, the range data size is reduced to $N_r = \Delta R_{bi}/c \cdot S_{rate}$, which alleviates the burden of communication subsystem. It should be noted that each element in the data matrix is a complex number, which contains real and imaginary parts in double type. As a result, the total size of the echo data matrix to be transmitted is $D_{echo}(d(i)) = 128N_a \cdot N_r$ in bits. The data size should be jointly considered with communication capacity of the UAV flight path to ensure complete transmission of echo data, which will be analyzed in the next subsection.

Last but not least, the data collection should not be obstructed by terrain. Thus, a constraint regarding imaging performance is introduced, *i.e.*, the line of sight from UAV platform to the target scene should be above the discrete terrain points.

C. Communication Performance with Ground Station

After echo collection and preprocessing, the data are transmitted to a ground-based processing station located at $GS(x_g, y_g, z_g)$. Suppose the communication link between UAV platform and ground station is line-of-sight link and Doppler effects due to UAV motion has been compensated.

For the discrete UAV flight path $d(i)$, the resulting channel can be expressed as a free-space path loss model as follows

$$h(d(i)) = \frac{\beta_0}{l^2(i)}, \quad (27)$$

where β_0 is the channel power at reference distance. $l(i) = \|P_i - GS\|$ is the distance between the UAV and ground station at the i th discrete way point. Based on the channel model, the instantaneous channel capacity at P_i can be formulated as

$$\begin{aligned} C(d(i)) &= B_{com} \cdot \log_2 \left(1 + \frac{P_{com}h(d(i))}{\sigma^2} \right) \\ &= B_{com} \cdot \log_2 \left(1 + \frac{P_{com}\beta_0}{\sigma^2 l^2(i)} \right) \text{ bit/second}, \end{aligned} \quad (28)$$

where B_{com} is the communication bandwidth. σ is the receiver Gaussian white noise power and P_{com} denotes the transmission power assumed to be constant during the path. The scaling factor $\beta_0 P_{com}/\sigma^2$ is the receiving signal to noise ratio at a reference distance, which is determined by the system parameters. It can be observed from (28) that the channel capacity is inversely proportional to the logarithm of the distance $l(i)$. Therefore, a flight path with a shorter distance to the ground station during data transmission can promote the channel capacity.

Let i_{com}^{start} and i_{com}^{end} denote the start and end indices of discrete path point in $d(i)$ corresponding to data transmission. The total amount of data bits being transmitted from the UAV to the ground station can be expressed as

$$D_{com}(d(i)) = \sum_{i=i_{com}^{start}}^{i_{com}^{end}} T(i) \cdot B_{com} \log_2 \left(1 + \frac{P_{com}\beta_0}{\sigma^2 l^2(i)} \right). \quad (29)$$

The UAV path should satisfy two constraints regarding communication performance. Firstly, line of sight link should be guaranteed between the UAV platform and ground station to fully exploit the channel capacity. Let N_{c4} denote the number of discrete points in the line of sight direction that is below the discrete terrain point. N_{c4} should be equal to zero to ensure no degradation of communication performance. On the other hand, the total amount of transmitted data $D_{com}(d(i))$ during the flight should be larger than the data size of echo signal $D_{echo}(d(i))$, *i.e.*, $D_{com}(d(i)) \geq D_{echo}(d(i))$, to make sure all the data are transmitted to the ground station.

In summary, the mission performance evaluators and constraints for the proposed passive UAV SAR system with a specific flight path $d(i)$ is summarized in Table II.

V. SIMULATION ANALYSIS AND PERFORMANCE VERIFICATION

In Section III, the passive UAV SAR system with different types of illuminators is analyzed in detail. The choice of illuminator determines the potential performance that can be achieved by the system. As analyzed in Section IV, the adopted UAV path is another crucial factor influencing the actual system performance, which should be considered in mission planning. Therefore, the mission performance in Table II and

TABLE II
SUMMARY OF MISSION PERFORMANCE EVALUATORS FOR PASSIVE UAV SAR SYSTEM.

Performance Evaluator	UAV Navigation	Passive SAR Imaging	Communication
Objective function	Energy consumption: $\min_{d(i)} E(d(i))$ Terrain threat: $\min_{d(i)} f_{\text{threat}}(d(i))$	Spatial resolution: $\min_{d(i)} \bar{S}_e(d(i))$	Transmitted Data Size: $\max_{d(i)} D_{\text{com}}(d(i))$
Constraints	Collision avoidance: $N_{c1} = 0$ Turning angle: $N_{c2} = 0$ $(N_{c2} \text{ is the number of discrete way points with turning angle larger than } \theta_{\max})$	Swath width: $W_r^{\text{Cov}} \geq W_r$ Data collection: $N_{c3} = 0$ $(N_{c3} \text{ is number of discrete points from UAV to target scene blocked by terrain})$	Data transmission: $N_{c4} = 0$ Mission data requirement: $D_{\text{com}}(d(i)) \geq D_{\text{echo}}(d(i))$

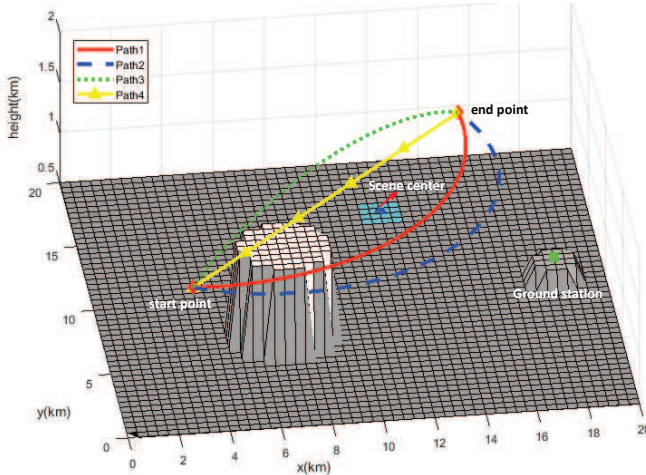


Fig. 5. Simulated scenario of passive UAV SAR system.

their characteristics are analyzed and verified by numerical simulations in this section.

The simulated working scenario of the passive UAV SAR system is illustrated in Fig. 5. A 3-D terrain with different elevations is generated within 20km extent both in x and y directions. The terrain contains the 'flat ground' with 500m altitude and two elevated areas in circular shape, one of which is located at (7, 7)km with 2km radius and 1.4km altitude and the other is located at (18, 10)km with 1km radius and 700m altitude. The interested target scene to be observed is located at (12, 16)km on the 'flat ground', which is marked by blue squares. The ground processing station is located at (18, 10, 0.72)km. In order to facilitate the analysis of mission performance, the coordinates of the start point and end point of the UAV paths are set as (3, 3.5, 1.5)km and (15, 15.6, 1.5)km, respectively.

Four potential UAV paths are generated for performance evaluation. Path 1 and path 2 are horizontal arcs connecting the start point and the end point with different radii. Path 4 is straight line path, which is also the chord of path 1 and path 2. The maximum horizontal distance is 4.01km between path 1 and path 4, and 6.16km between path 2 and path 4. As the heights of the start point and end point are the same, path 1,

path 2 and path 4 are level flight without vertical motion. In order to evaluate the energy consumption of UAV with 3-D motion, path 3 is modeled as a vertical arc with maximum height difference of 400m compared with path 4. Path 3 and path 4 have the same ground projection on xy plane.

TABLE III
SIMULATED PARAMETERS OF PASSIVE UAV SAR SYSTEM.

UAV platform			
UAV mass (m)	40kg	Parasitic drag factor(c_1)	9.36×10^{-4}
Bandwidth(B_{com})	10MHz	Lift-induced drag factor(c_2)	2250
Reference SNR(SNR_{ref})	70dB	Elevation antenna size(d_{el})	0.5m
Platform velocity (v)	50m/s	Azimuth antenna size(d_{az})	1.2m
Sampled targets(N_s)	25	Discrete path point(N_{dp})	1000
Safe distance(r_{safe})	200m	Range sampling rate(S_{rate})	120MHz
Illuminator			
Inclination	53°	Semi-major axis	42164km
Eccentricity	0.07	Argument of perigee	270°
PRF	100Hz	Off nadir angle	6°

Assume that the observation mission requires $2m \times 2m$ spatial resolution within 1km swath width. According to the analysis in Section III, the SAR illuminators can achieve the required imaging performance, including LEO, MEO and GEO-SAR satellites. Based on the parameter settings, the minimum distance of the potential path is 17.04km, which corresponds to 341 seconds flight time. In order to facilitate the signal synchronization between the illuminator and the UAV receiver, a longer beam coverage time of the illuminator is desired to guarantee the signal accessibility during the flight. Therefore, in the following simulation, a GEO-SAR satellite is considered as the illuminator for the passive UAV SAR system. The simulation parameters of the passive UAV SAR system are given in Table. III. 25 sample point targets are chosen to evaluate the spatial resolution of a path, which are evenly distributed in the 1km imaging swath described in Section IV. It should be noted that the SAR signal collecting window is centered at the mid-point of each path, which is also the starting position of communication with ground station.

TABLE IV
MISSION PERFORMANCE OF THE SIMULATED PATHS.

Performance	Length(km)	E (J)	f_{threat}	\bar{S}_c (m^2)	D_{echo} (bit)	D_{com} (bit)
Path 1	19.46	6.31×10^4	735.3	3.49	2.99×10^8	1.09×10^9
Path 2	22.45	7.27×10^4	735.9	3.04	3.63×10^8	1.98×10^9
Path 3	17.07	2.13×10^5	903.1	8.90	3.27×10^8	4.84×10^8
Path 4	17.04	5.52×10^4	2186.8	8.75	3.29×10^8	4.83×10^8

The mission performance of the four paths in the simulated scenario is illustrated in Table IV, where path length is also listed for comparison. The mission performance of the four UAV paths in the simulated scenario is analyzed and verified in three aspects in the following.

UAV navigation: The navigation performance of a UAV path is mainly composed of energy consumption, terrain threat and path length, which is generally considered in the current literature. It can be observed from Table IV that the straight-line path, *i.e.*, path 4, presents the shortest path length while path 2 is the longest with 22.45km. The path length increases when the UAV makes a further detour during the flight, which can be inferred from Fig. 5. When the UAV platform is engaged in steady level flight with no vertical motion, *i.e.*, path 4, path 1 and path 2, the energy consumption, E , approximately linearly increases with path length, which means the energy consumption can represent the length performance of a path. However, although the lengths of path 3 is only 0.03km longer than that of path 4, the energy consumption is significantly larger due to the climbing motion of UAV platform. Therefore, climbing will introduce additional energy consumption and should be considered in mission planning for the passive UAV SAR system. On the other hand, the threat value, f_{threat} , is calculated using the distance between the discrete path points and their surrounding terrain points. It can be observed that path 4 has the largest threat value, which directly traverses the elevated area and parts of the path is close to the terrain obstacles in Fig. 5. Path 1 and path 2 make different detours in horizontal direction to avoid the elevated area and significantly reduce the threat value, which is preferable for safe navigation. For path 3, although it still flies through the elevation, the path keeps a safe distance with the terrain obstacles and achieves a satisfactory threat value by increasing the flight altitude. Therefore, it can be concluded from the above analysis that a 'smoother' path with less maneuvers in elevation direction is desired for energy-efficient UAV SAR mission. Moreover, the path should keep enough distance from the terrain obstacles to guarantee the safe navigation for UAV platform.

Passive SAR imaging: From Table IV, path 1 and path 2 can provide better imaging performance compared with path 3 and path 4. In order to analyze and verify the imaging performance, SAR raw-data simulations are conducted in this section for each UAV path listed in Table IV. 25 ideal point targets are evenly distributed in the $1\text{km} \times 1\text{km}$ imaging scene for performance evaluation, which correspond to the sampled

targets engaged in the calculation of \bar{S}_c . From Figs. 6 to 9, the imaging results of passive UAV SAR raw data processed by BPA are illustrated with respect to the paths. For each path, the imaging result of the 25 point targets in the whole scene is shown on the left, with zoomed in view of the selected targets on the right. The selected targets include the reference point 'Ref.' and the targets with minimum and maximum S_c , denoted as 'Min.' and 'Max.', respectively. The coordinates of the selected targets are given and the contours of the imaging results are plotted within $16\text{m} \times 12\text{m}$ ground xy plane.

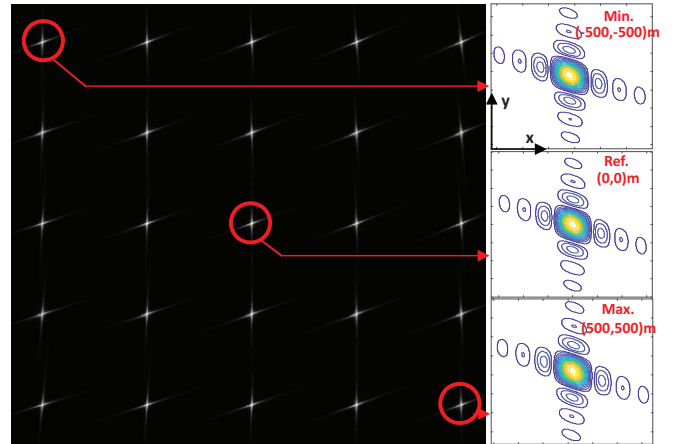


Fig. 6. Imaging result of path 1.

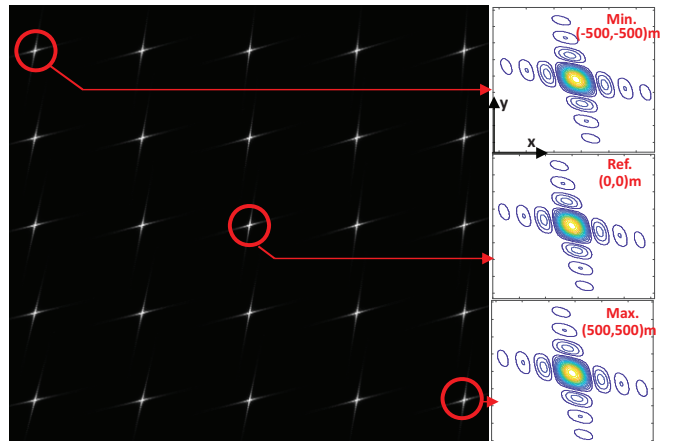


Fig. 7. Imaging result of path 2.

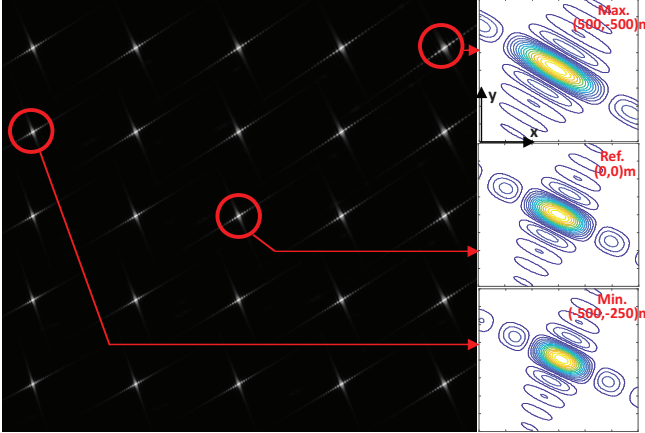


Fig. 8. Imaging result of path 3.

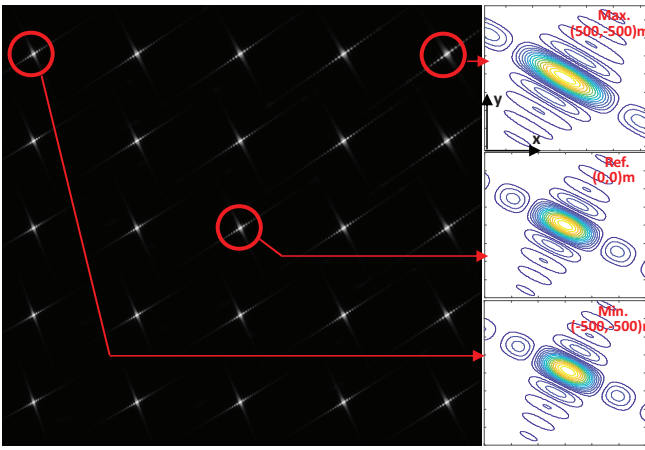


Fig. 9. Imaging result of path 4.

It can be observed from Figs. 6 to 9 that the spatial resolution is varied with respect to target coordinates. The positions of targets with maximum and minimum S_c are different among the imaging results of the four simulated paths. Therefore, it can be concluded that resolution and its spatial variance are dependent on the bi-static observation geometry, which is determined by the adopted paths. Moreover, from Figs. 6 to 9, path 3 and path 4 are inferior to path 1 and path 2 regarding spatial resolution performance, with larger impulse response areas in the contour plots of the selected targets. The 3dB impulse response widths (IRW) of the selected point targets are measured according to the imaging results, which is shown in Table V. The measured S_c is calculated by (10) using the azimuth and range IRW and resolution direction angle α_D in Table V. The measured S_c s are close to the theoretical values, which verifies the derivations in Subsection III-A. The spatial resolutions achieved by path 1 and path 2 are finer than $2m \times 2m$ in the $1km \times 1km$ imaging scene, which can satisfy the mission requirements. However, for path 3 and path 4, the azimuth IRWs of the selected targets exceed 2m and the resulting S_c is significantly coarsened. On the other hand, the disequilibrium factors, S_c^{\max}/S_c^{\min} , of path 1 and path 2 are 1.20 and 1.12, respectively, which are much smaller

compared with path 3 (1.60) and path 4 (1.60). Therefore, the spatial variances of resolution for path 1 and path 2 are less significant than those of path 3 and path 4, which provides more consistent imaging performance for targets in the whole scene.

TABLE V
MEASURED IMAGING METRICS OF THE SELECTED TARGETS.

Imaging performance		Path 1	Path 2	Path 3	Path 4
Ref.	IRW ^R (m)	1.72	1.78	1.61	1.60
	IRW ^A (m)	1.55	1.36	3.20	3.21
	α_D (°)	113	116	108	105
	Measured S_c (m ²)	2.89	2.69	5.42	5.32
	S_c^{ref} (m ²)	2.90	2.71	5.44	5.34
Max.	IRW ^R (m)	1.70	1.75	1.59	1.58
	IRW ^A (m)	1.73	1.48	4.28	4.32
	α_D (°)	112	115	109	105
	Measured S_c (m ²)	3.17	2.86	7.20	7.07
	S_c^{\max} (m ²)	3.18	2.87	7.23	7.09
Min.	IRW ^R (m)	1.74	1.82	1.62	1.61
	IRW ^A (m)	1.39	1.26	2.62	2.63
	α_D (°)	114	118	110	107
	Measured S_c (m ²)	2.65	2.57	4.52	4.43
	S_c^{\min} (m ²)	2.66	2.56	4.52	4.43

Communication: Inspecting Table IV, all of the four paths can completely transmit the echo data to the ground processing station, which satisfy the mission data requirement constraint in Table II. However, path 1 and path 2 can provide better communication performance with higher data transmission capacity compared with path 3 and path 4. The abundance of communication capacity enables more mission opportunities during the flight, such as synchronization data transmission, online flight control, additional observation task and data retransmission. As analyzed in Subsection IV-C, shorter distance between the UAV platform and ground station can enhance the communication performance. It can be observed from Fig. 5 that the detours of path 1 and path 2 have shorten the distance between the path and the ground station, which verifies the superiority of communication performance evidenced in Table II.

Based on the above analysis, path 1 can provide a better overall mission performance, with satisfactory imaging performance, energy efficiency and safety. Path 2, on the other hand, can achieve even better imaging and communication performance at the cost of longer path and more energy consumption. Both paths can be adopted to accomplish the simulated passive UAV SAR mission.

VI. CONCLUSION AND FUTURE WORK

In this paper, an energy-efficient passive UAV SAR system using illuminators of opportunity is put forward. During the flight mission, the UAV platform passively receives the echo of the illuminator and transmit the data to a ground station after onboard preprocessing, where imaging processing and further

target recognition are accomplished. The system concept and block diagram are firstly analyzed, which is composed of three subsystems, *i.e.*, the navigation, communication and SAR processing subsystems. The spatial resolution of the system is then analyzed based on imaging geometry and extended gradient method. Then, the imaging performance and feasibility of the system with different kinds of illuminators are analyzed and compared, including spatial resolution and radiometric performance. It is found that the flight path of the UAV platform is a crucial factor influencing the mission performance of the whole system. In order to comprehensively evaluate the performance of the proposed system, the relationship between the UAV path and mission performance are analyzed thoroughly and the corresponding evaluators are put forward. Finally, the mission performance evaluators are analyzed and verified by numerical simulations in a 3-D terrain environment, which can accurately represent the system performance and lays the theoretical foundation for mission planning.

The proposed evaluator set quantitatively establishes the relationship between the mission performance and adopted UAV path in 3-D terrain environments. Based on the evaluator set, the mission planning for the energy-efficient UAV radar imaging system aiming at generating a flight plan that can safely guide the UAV platform to travel through the 3-D terrain and achieve optimized imaging and communication performance during the flight will be our future work.

REFERENCES

- [1] C. A. Wiley, "Synthetic aperture radars," *IEEE Trans. Aerosp. Electron. Syst.*, vol. 21, no. 3, pp. 440–443, 1985.
- [2] A. Moreira, P. Prats-Iraola, M. Younis, G. Krieger, I. Hajnsek, and K. P. Papathanassiou, "A tutorial on synthetic aperture radar," *IEEE Geosci. Remote Sens. Mag.*, vol. 1, no. 1, pp. 6–43, 2013.
- [3] I. G. Cumming and F. H. Wong, "Digital processing of synthetic aperture radar data," *Artech house*, vol. 1, no. 3, 2005.
- [4] C. Hu, Z. Chen, X. Dong, and C. Cui, "Multistatic geosynchronous SAR resolution analysis and grating lobe suppression based on array spatial ambiguity function," *IEEE Trans. Geosci. Remote Sens.*, vol. PP, no. 99, pp. 1–19, 2020.
- [5] Z. Sun, J. Wu, J. Pei, Z. Li, Y. Huang, and J. Yang, "Inclined geosynchronous spaceborneairborne bistatic SAR: Performance analysis and mission design," *IEEE Trans. Geosci. Remote Sens.*, vol. 54, no. 1, 2016.
- [6] J. Wu, Z. Sun, H. An, J. Qu, and J. Yang, "Azimuth signal multichannel reconstruction and channel configuration design for geosynchronous spaceborneairborne bistatic SAR," *IEEE Trans. Geosci. Remote Sens.*, vol. 57, no. 4, pp. 1861–1872, 2019.
- [7] G. Krieger, I. Hajnsek, K. P. Papathanassiou, M. Younis, and A. Moreira, "Interferometric synthetic aperture radar (SAR) missions employing formation flying," *Proc. IEEE*, vol. 98, no. 5, pp. 816–843, 2010.
- [8] S. Huber, F. Q. de Almeida, M. Villano, M. Younis, G. Krieger, and A. Moreira, "Tandem-I: A technical perspective on future spaceborne SAR sensors for earth observation," *IEEE Trans. Geosci. Remote Sens.*, vol. 56, no. 8, pp. 4792–4807, 2018.
- [9] F. Xue, X. Wang, F. Xu, and Y. Wang, "Polarimetric SAR interferometry: A tutorial for analyzing system parameters," *IEEE Geosci. Remote Sens. Mag.*, vol. 8, no. 2, pp. 83–107, 2020.
- [10] Z. Sun, J. Wu, Z. Li, H. An, and X. He, "Geosynchronous spaceborne-airborne bistatic SAR data focusing using a novel range model based on one-stationary equivalence," *IEEE Trans. Geosci. Remote Sens.*, pp. 1–17, 2020.
- [11] H. An, J. Wu, Z. Sun, and J. Yang, "A two-step nonlinear chirp scaling method for multichannel GEO spaceborneairborne bistatic SAR spectrum reconstructing and focusing," *IEEE Trans. Geosci. Remote Sens.*, vol. 57, no. 6, pp. 3713–3728, 2019.
- [12] Z. Li, S. Li, Z. Liu, H. Yang, J. Wu, and J. Yang, "Bistatic forward-looking SAR MP-DPCA method for space-time extension clutter suppression," *IEEE Trans. Geosci. Remote Sens.*, pp. 1–15, 2020.
- [13] P. Huang, X.-G. Xia, X. Liu, and G. Liao, "Refocusing and motion parameter estimation for ground moving targets based on improved axis rotation-time reversal transform," *IEEE Trans. Comput. Imag.*, vol. 4, no. 3, pp. 479–494, 2020.
- [14] W. Pitz and D. Miller, "The terrasar-x satellite," *IEEE Trans. Geosci. Remote Sens.*, vol. 48, no. 2, pp. 615–622, 2010.
- [15] S. Hobbs, C. Mitchell, B. Forte, R. Holley, B. Snapir, and P. Whittaker, "System design for geosynchronous synthetic aperture radar missions," *IEEE Trans. Geosci. Remote Sens.*, vol. 52, no. 12, pp. 7750–7763, 2014.
- [16] J. Matar, M. Rodriguez-Cassola, G. Krieger, P. Lpez-Dekker, and A. Moreira, "MEO SAR: System concepts and analysis," *IEEE Trans. Geosci. Remote Sens.*, vol. 58, no. 2, pp. 1313–1324, 2020.
- [17] A. Liu, F. Wang, H. Xu, and L. Li, "N-SAR: A new multichannel multimode polarimetric airborne SAR," *IEEE J. Sel. Topics Appl. Earth Observ. Remote Sens.*, 2018.
- [18] N. Gebert, F. Queiroz de Almeida, and G. Krieger, "Airborne demonstration of multichannel SAR imaging," *IEEE Geosci. Remote Sens. Lett.*, vol. 8, no. 5, pp. 963–967, 2011.
- [19] J. Saeedi, "Feasibility study and conceptual design of missile-borne synthetic aperture radar," *IEEE Trans. Syst., Man, Cybern., Syst.*, vol. 50, no. 3, pp. 1122–1133, 2020.
- [20] S. Chen, S. Zhang, H. Zhao, and Y. Chen, "A new chirp scaling algorithm for highly squinted missile-borne SAR based on frft," *IEEE J. Sel. Topics Appl. Earth Observ. Remote Sens.*, vol. 8, no. 8, pp. 3977–3987, 2015.
- [21] D. Feng, D. An, and X. Huang, "An extended fast factorized back projection algorithm for missile-borne bistatic forward-looking SAR imaging," *IEEE Trans. Aerosp. Electron. Syst.*, vol. 54, no. 6, pp. 2724–2734, 2018.
- [22] P. E. Hart, N. J. Nilsson, and B. Raphael, "A formal basis for the heuristic determination of minimum cost paths," *IEEE Trans. Syst. Sci. Cybern.*, vol. 4, no. 2, pp. 100–107, 1968.
- [23] I. K. Nikolos, K. P. Valavanis, N. C. Tsourveloudis, and A. N. Kostaras, "Evolutionary algorithm based offline/online path planner for UAV navigation," *IEEE Trans. Syst., Man, Cybern. B, Cybern.*, vol. 33, no. 6, pp. 898–912, 2003.
- [24] S. Mittal and K. Deb, "Three-dimensional offline path planning for UAVs using multiobjective evolutionary algorithms," in *Proc. Congr. Evol. Comput.* Singapore, 2007, pp. 3195–3202.
- [25] A. Garcia-Rodriguez, G. Geraci, D. Lopez-Perez, L. G. Giordano, M. Ding, and E. Bjornson, "The essential guide to realizing 5g-connected UAVs with massive MIMO," *IEEE Commun. Mag.*, vol. 57, no. 12, pp. 84–90, 2019.
- [26] Y. Wang, Z. Ru, K. Wang, and P. Huang, "Joint deployment and task scheduling optimization for large-scale mobile users in multi-UAV-enabled mobile edge computing," *IEEE Trans. Cybern.*, pp. 1–14, 2019.
- [27] C. C. Murray and W. Park, "Incorporating human factor considerations in unmanned aerial vehicle routing," *IEEE Trans. Syst., Man, Cybern. Syst.*, vol. 43, no. 4, pp. 860–874, 2013.
- [28] L. Lin and M. A. Goodrich, "Hierarchical heuristic search using a gaussian mixture model for UAV coverage planning," *IEEE Trans. Cybern.*, vol. 44, no. 12, pp. 2532–2544, 2014.
- [29] S. Minaeian, J. Liu, and Y. Son, "Vision-based target detection and localization via a team of cooperative UAV and UGVs," *IEEE Trans. Syst., Man, Cybern. Syst.*, vol. 46, no. 7, pp. 1005–1016, 2016.
- [30] D. Avola, L. Cinque, G. L. Foresti, N. Martinel, D. Pannone, and C. Piciarelli, "A UAV video dataset for mosaicking and change detection from low-altitude flights," *IEEE Trans. Syst., Man, Cybern. Syst.*, vol. 50, no. 6, pp. 2139–2149, 2020.
- [31] H. Sedjelmaci, S. M. Senouci, and N. Ansari, "A hierarchical detection and response system to enhance security against lethal cyber-attacks in UAV networks," *IEEE Trans. Syst., Man, Cybern. Syst.*, vol. 48, no. 9, pp. 1594–1606, 2018.
- [32] W. Wang, Q. Peng, and J. Cai, "Waveform-diversity-based millimeter-wave UAV SAR remote sensing," *IEEE Trans. Geosci. Remote Sens.*, vol. 47, no. 3, pp. 691–700, 2009.
- [33] S. Lentilhac, "UAV flight plan optimzed for sensor requirements," *IEEE Aerosp. Electron. Syst. Mag.*, vol. 25, no. 2, pp. 11–14, 2010.
- [34] X. Yan, S. Member, J. Chen, B. Liyanage, P. Wang, and W. Yang, "A light-weight SAR system for multi-rotor UAV platform using LFM quasi-cw waveform," in *Proc. IEEE IGARSS*, 2016, pp. 7346–7349.
- [35] J. D. Coker and A. H. Tewfik, "Performance synthesis of UAV trajectories in multistatic SAR," *IEEE Trans. Aerosp. Electron. Syst.*, vol. 47, no. 2, pp. 848–863, 2011.

[36] M. Lort, A. Aguasca, C. Lpez-Martnez, and T. M. Marl, "Initial evaluation of SAR capabilities in UAV multicopter platforms," *IEEE J. Sel. Topics Appl. Earth Observ. Remote Sens.*, vol. 11, no. 1, pp. 127–140, 2018.

[37] L. Zhang, J. Sheng, M. Xing, Z. Qiao, T. Xiong, and Z. Bao, "Wavenumber-domain autofocusing for highly squinted UAV SAR imagery," *IEEE Sensors J.*, vol. 12, no. 5, pp. 1574–1588, 2012.

[38] S. Zhou, L. Yang, L. Zhao, and G. Bi, "Quasi-polar-based FFBP algorithm for miniature UAV SAR imaging without navigational data," *IEEE Trans. Geosci. Remote Sens.*, vol. 55, no. 12, pp. 7053–7065, 2017.

[39] L. Zhang, Z. Qiao, M. Xing, L. Yang, and Z. Bao, "A robust motion compensation approach for UAV SAR imagery," *IEEE Trans. Geosci. Remote Sens.*, vol. 50, no. 8, pp. 3202–3218, 2012.

[40] D. You, G. Sun, X. Xia, M. Xing, Y. Li, B. Li, and Z. Bao, "Time-varying baseline error estimation and compensation in UAV SAR interferometry based on time-domain subaperture of raw radar data," *IEEE Sensors J.*, pp. 1–1, 2020.

[41] M. Xing, X. Jiang, R. Wu, F. Zhou, and Z. Bao, "Motion compensation for UAV SAR based on raw radar data," *IEEE Trans. Geosci. Remote Sens.*, vol. 47, no. 8, pp. 2870–2883, 2009.

[42] Y. Fang, G. Atkinson, A. Sayin, J. Chen, P. Wang, M. Antoniou, and M. Cherniakov, "Improved passive SAR imaging with DVB-T transmissions," *IEEE Trans. Geosci. Remote Sens.*, vol. 58, no. 7, pp. 5066–5076, 2020.

[43] T. Zeng, T. Zhang, W. Tian, and C. Hu, "Space-surface bistatic SAR image enhancement based on repeat-pass coherent fusion with beidou-2/compass-2 as illuminators," *IEEE Geosci. Remote Sens. Lett.*, vol. 13, no. 12, pp. 1832–1836, 2016.

[44] B. Yonet, E. Mason, and B. Yazici, "Deep learning for passive synthetic aperture radar," *IEEE J. Select. Topics Signal Process.*, vol. 12, no. 1, pp. 90–103, 2018.

[45] J. R. Gutierrez Del Arroyo and J. A. Jackson, "WiMAX OFDM for passive SAR ground imaging," *IEEE Trans. Aerosp. Electron. Syst.*, vol. 49, no. 2, pp. 945–959, 2013.

[46] D. Gromek, K. Radecki, J. Drozdowicz, P. Samczyski, and J. Szabatin, "Passive SAR imaging using DVB-T illumination for airborne applications," *IET Radar, Sonar Navigat.*, vol. 13, no. 2, pp. 213–221, 2019.

[47] Z. Sun, J. Wu, J. Yang, Y. Huang, C. Li, and D. Li, "Path planning for GEO-UAV bistatic SAR using constrained adaptive multiobjective differential evolution," *IEEE Trans. Geosci. Remote Sens.*, vol. 54, no. 11, pp. 6444–6457, 2016.

[48] Q. Zhang, Z. Dong, Y. Zhang, and Z. He, "GEO-UAV bistatic circular synthetic aperture radar: Concepts and technologies," in *Proc. IEEE IGARSS*, 2016, pp. 4195–4198.

[49] M. Antoniou and M. Cherniakov, "GNSS-based bistatic SAR: a signal processing view," *EURASIP J. Adv. Signal Process.*, vol. 2013, no. 1, pp. 1–16, 2013.

[50] H. Ma, M. Antoniou, and M. Cherniakov, "Passive GNSS-based SAR resolution improvement using joint galileo E5 signals," *IEEE Geosci. Remote Sens. Lett.*, vol. 12, no. 8, pp. 1640–1644, 2015.

[51] L. Zhang, H. Li, Z. Qiao, M. Xing, and Z. Bao, "Integrating autofocus techniques with fast factorized back-projection for high-resolution spotlight SAR imaging," *IEEE Geosci. Remote Sens. Lett.*, vol. 10, no. 6, pp. 1394–1398, 2013.

[52] A. Moccia and A. Renga, "Spatial resolution of bistatic synthetic aperture radar: Impact of acquisition geometry on imaging performance," *IEEE Trans. Geosci. Remote Sens.*, vol. 49, no. 10, pp. 3487–3503, 2011.

[53] Junjie Wu, Jianyu Yang, Yulin Huang, Haiguang Yang, and Haocheng Wang, "Bistatic forward-looking SAR: Theory and challenges," in *Proc. IEEE Radar Conf.*, 2009, pp. 1–4.

[54] N. Gebert, G. Krieger, and A. Moreira, "Digital beamforming on receive: Techniques and optimization strategies for high-resolution wide-swath SAR imaging," *IEEE Trans. Aerosp. Electron. Syst.*, vol. 45, no. 2, pp. 564–592, 2009.

[55] F. Liu, M. Antoniou, Z. Zeng, and M. Cherniakov, "Coherent change detection using passive GNSS-based BSAR: Experimental proof of concept," *IEEE Trans. Geosci. Remote Sens.*, vol. 51, no. 8, pp. 4544–4555, 2013.

[56] F. Santi, M. Antoniou, and D. Pastina, "Point spread function analysis for GNSS-based multistatic SAR," *IEEE Geosci. Remote Sens. Lett.*, vol. 12, no. 2, pp. 304–308, 2015.

[57] Y. Fu, M. Ding, C. Zhou, and H. Hu, "Route planning for unmanned aerial vehicle (UAV) on the sea using hybrid differential evolution and quantum-behaved particle swarm optimization," *IEEE Trans. Syst., Man, Cybern., Syst.*, vol. 43, no. 6, pp. 1451–1465, 2013.

[58] Changwen Zheng, Lei Li, Fanjiang Xu, Fuchun Sun, and Mingyue Ding, "Evolutionary route planner for unmanned air vehicles," *IEEE Trans. Robot.*, vol. 21, no. 4, pp. 609–620, 2005.

[59] I. K. Nikolos, K. P. Valavanis, N. C. Tsourveloudis, and A. N. Kostaras, "Evolutionary algorithm based offline/online path planner for UAV navigation," *IEEE Trans. Syst., Man, Cybern. B, Cybern.*, vol. 33, no. 6, pp. 898–912, 2003.

[60] Y. Zeng and R. Zhang, "Energy-efficient UAV communication with trajectory optimization," *IEEE Trans. Wireless Commun.*, vol. 16, no. 6, pp. 3747–3760, 2017.

[61] Q. Zhang, J. Wu, C. Li, J. Yang, Y. Huang, H. Yang, and X. Yang, "Study of the effects of non-square resolutions of bistatic sar on template matching performance," in *Proc. IEEE IGARSS*, 2018, pp. 557–560.